RESEARCH ARTICLE

Check for updates

Enhancing photoluminescence efficiency of atomically precise copper(I) nanoclusters through a solvent-induced structural transformation†

Su-Kao Peng, [ID] ‡ Hu Yang, [ID] ‡ Dong Luo, [ID] Mo Xie, [ID] Wen-Jing Tang, [ID] Guo-Hong Ning [ID] * and Dan Li [ID] *

Atomically precise copper(I) nanoclusters (CuNCs) with high photoluminescence (PL) efficiency and a relatively short lifetime could be promising non-precious metal-based phosphorescent emitters for organic light-emitting diodes (OLEDs), but the synthesis of such CuNCs still remains a great challenge. Herein, we have prepared a parallelepiped-like and green emissive atomically precise **Cu₁₀** alkynyl cluster with a moderate PLQY of 35% and lifetime (τ_{av}) of 8.4 μs. Interestingly, upon addition of hexane to a DCM solution of **Cu₁₀**, it turns into an hourglass-like, orange emissive **Cu₁₈** cluster with an enhanced PL efficiency (PLQY = 63%, and τ_{av} = 2.8 μs) at room temperature, which is rarely achieved in high-nuclearity alkynyl-protected CuNCs. Experiments and theoretical calculations suggested that the excellent PL performance of **Cu₁₈** is due to reduced nonradiative transition, a larger d orbital contribution of Cu ions, an enhanced transition dipole moment and reduced HOMO–LUMO gap. This work will not only pave a novel approach for constructing alkynyl-protected CuNCs with a high PLQY and short lifetime, which might be explored for other CuNCs for fabricating high-performance OLEDs, but also shed light on the structure–luminescence relationship.

Introduction

Atomically precise coinage metal clusters, with a well-defined structure and discrete energy levels,[1–3] have drawn extensive attention in many research fields including photolumines-

College of Chemistry and Materials Science, Guangdong Provincial Key Laboratory of Functional Supramolecular Coordination Materials and Applications, Jinan University, Guangzhou 510632, China. E-mail: guohongning@jnu.edu.cn, danli@jnu.edu.cn

cent materials,[4–7] chirality,[8–10] catalysis,[11–13] sensing[14–16] and biomedicine.[17,18] In the past decade, many synthetic strategies were developed for constructing Au/Ag nanoclusters (Au/AgNCs) with excellent photoluminescence (PL) properties and several kinds of ligands have been employed as protecting groups such as thiols, phosphines and alkynes.[1,19] Compared to the well-established Au/AgNCs, the isolation of Cu nanoclusters (CuNCs) with high PL efficiency is highly challenging due to the unstable nature of Cu(I) toward O₂. Moreover, thiol and phosphine ligands are conventionally used as protecting ligands to fabricate CuNCs, but only a few atomically precise alkynyl-protected CuNCs have been synthesized.[5]

Dr Guo-Hong Ning is currently a professor in the College of Chemistry and Materials Science at Jinan University. He obtained his Ph.D. from the University of Tokyo under the supervision of Prof. Makoto Fujita. During 2013–2015, he held a JSPS postdoctoral fellowship at the University of Tokyo, working with Prof. Makoto Fujita. Prior to joining Jinan University, he worked as a postdoctoral associate with Prof. Loh Kian Ping at the National University of Singapore (2015–2017) and with Prof. Andrew I. Cooper (FRS) at the University of Liverpool (2017–2018). His primary research interests focus on function- led porous crystalline materials, including metal–organic frameworks (MOFs), covalent–organic frameworks (COFs), and the recently developed cyclic trinuclear complex-based MOFs by combining the chemistry of MOFs and COFs. He has published more than 40 peer-reviewed papers including in Nature Energy, Nature Chemistry, Nature Communications, Journal of the American Chemical Society, Angewandte Chemie International Edition, and so on. In the past year, he has published three important papers in Inorganic Chemistry Frontiers.

This journal is © the Partner Organisations 2022

Inorg. Chem. Front., 2022, **9**, 5327–5334 | 5327

Phosphorescent emitters show great potential for organic light-emitting diodes (OLEDs) due to their much higher internal quantum efficiency (IQE) (~100%) compared to that of fluorescent emitters (less than 25% IQE). Due to the large spin–orbit coupling (SOC) parameter (ξ) and the fast rate of intersystem crossing (ISC) ($k > 10^5$ s^{-1}) of noble metal (*e.g.*, Ir and Pt) emitters,[20] they might be promising for commercial applications; however, their scarcity and toxicity have hampered further applications. Therefore, the development of less toxic and non-precious metal-based (*i.e.*, copper) phosphorescent emitters with a high PL quantum yield (PLQY) and a relatively short lifetime (of approx. μs) at room temperature (rt) is

highly desired for OLEDs.[21] Since the copper nucleus has a smaller ξ and a slower rate of ISC ($k = 10^3$ to 10^5 s^{-1}) than those of noble metals, it is hard for copper-based phosphorescent emitters to achieve a high PLQY and short lifetime. Although a few reported examples of CuNCs protected with phosphine[22] or thiol ligands[23] have realized a high PLQY and been used for OLEDs, the alkynyl-protected CuNCs still display a weak PLQY at rt (Fig. 1).[10]

Due to adjustable π-acidity/basicity and decorated reaction sites in the ligand,[24,25] coinage metal-based cyclic trinuclear complexes (CTCs) can serve as initial reaction species or second building units to construct a series of clusters,[26–28] cages,[29,30] and coordination polymers.[31–33] More recently, by reacting Ag$_3$[3,5-(CF$_3$)$_2$Pz]$_3$ with phenylacetylene, our group first reported weakly emissive alkynyl-protected AgNCs with noria-like structures. After doping with Cu/Au ions, a class of brightly phosphorescent Ag/Cu or Au/Ag alloy clusters were afforded (Scheme 1a).[26,28] Inspired by this, we envisioned that atomically precise alkynyl-protected CuNCs with a high PLQY can be readily prepared by the reaction between Cu-CTCs and alkyne ligands. Herein, we report a bright green emissive, anion parallelepiped-like alkynyl-protected CuNC (**Cu$_{10}$**) by reacting Cu$_3$Pz$_3$ (Pz = 3,5-bis-(trifluoromethyl)-pyrazolate) with phenylacetylene in the presence of triethylamine. Subsequently, the addition of hexane to the dichloromethane (DCM) solution of **Cu$_{10}$** would induce structural transformation and yield an hourglass-like, neutral orange emissive CuNC (**Cu$_{18}$**) (Scheme 1b). Interestingly, **Cu$_{18}$** exhibited a lower emission wavelength, higher PLQY (63%), short lifetime (τ_{av} = 2.8 μs), and quicker radiative decay rate (k_r = 2.2 × 10^5 s^{-1}) than those of **Cu$_{10}$** (PLQY of 35%, τ_{av} = 8.4 μs and k_r = 6.9 × 10^4 s^{-1}) at rt. Computational investigations were
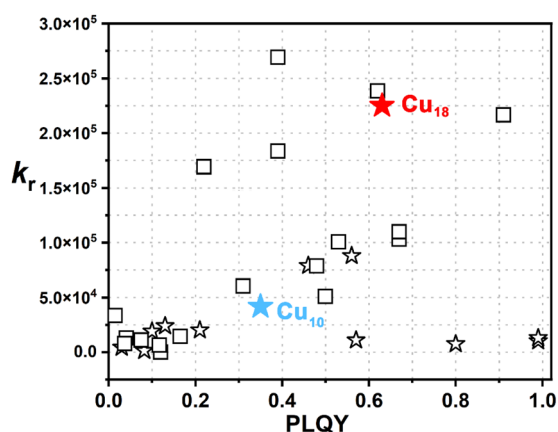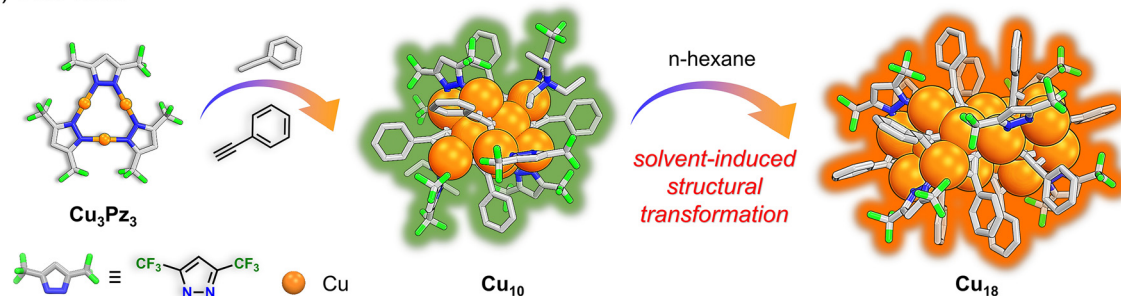

Fig. 1 Summary of calculated radiative decay rate ($k_r = \Phi/\tau$) *versus* PLQY (Φ) of all reported atomically precise CuNCs, including protected S$^-$, P$^-$ and I$^-$ ligands (squares) and C≡C$^-$ (pentagons) (see Table S5† for details).
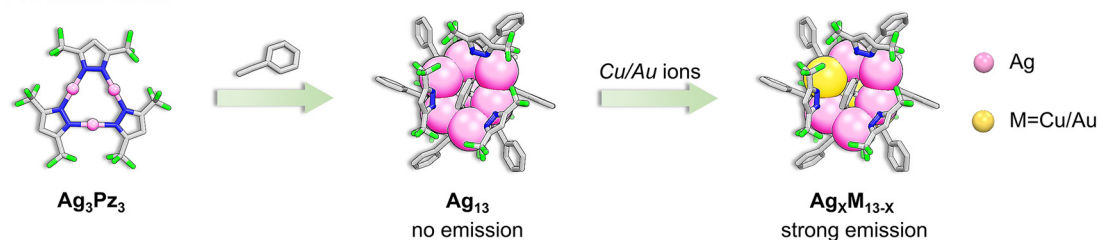
Scheme 1 The schematic diagram showing (a) the synthesis of **Ag$_{13}$** and an Au−Ag/Cu−Ag bimetallic cluster obtained by a doping strategy, and (b) the formation of **Cu$_{10}$** and **Cu$_{18}$** *via* a solvent-induced structural transformation.

conducted to reveal the photophysical mechanism of Cu_{10} and Cu_{18}, and the superior PL properties of Cu_{18} are attributed to the larger d orbital contribution of Cu ions, enhanced transition dipole moment and reduced HOMO–LUMO gap compared to Cu_{10}. More importantly, the reduced nonradiative transition, high PLQY, short lifetime and fast rate of ISC (comparable to that of Ir and Pt emitters) of Cu_{18} demonstrated a rare case of CuNCs that might have potential application for OLEDs. Our studies pave a novel approach for constructing alkyne CuNCs with a high PLQY and suitable lifetime in the range of sub-μs to μs, which might be explored for other CuNCs when fabricating high-performance OLEDs.

Experimental section

Preparation of $[Cu(3,5\text{-}(CF_3)_2\text{-}Pz)]_3$ (Cu_3Pz_3)

Cu_3Pz_3 was synthesized following the literature methods.[28,34]

Preparation of Cu_{10}

Cu_3Pz_3 (0.3 mmol, 240 mg) was dissolved in 8 mL of DCM under a nitrogen atmosphere. After 30 min, 0.6 mL of phenylacetylene and 0.6 mL of NEt_3 were added under vigorous stirring at rt. Then, the solution turned yellow and continued to be stirred for 2 hours. The resultant solution was left to evaporate slowly in the dark at −20 °C overnight, yielding yellow-green block crystals. Yield: 90% (based on Cu). Elemental analysis (%) for $C_{93}H_{74}Cl_6Cu_{10}F_{36}N_{14}$, found (calcd): C, 40.55 (40.59); H, 2.47 (2.50); N, 7.35 (7.36).

Preparation of Cu_{18}

Cu_{10} (0.0056 mmol, 15 mg) was dissolved in 1 mL of DCM, then 29 mL of n-hexane was added. The mixture solution was left to stand in the dark at −20 °C for five days to afford orange block crystals. Yield: 60.0% (based on Cu). Elemental analysis (%) for $C_{127}H_{68}ClCu_{18}F_{36}N_{12}$, found (calcd): C, 42.35 (42.32); H, 1.89 (1.86); N, 4.66 (4.70).

Results and discussion

Synthesis, characterization and structures

The Cu-CTC (Cu_3Pz_3) was synthesized according to previous reports.[28,34] The mixture of Cu_3Pz_3, phenylacetylene and triethylamine (Et_3N) in the DCM solvent at rt under a N_2 atmosphere produced a yellow solution, and subsequently, high-quality yellow-green block crystals of the Cu_{10} cluster suitable for single-crystal X-ray diffraction (SCXRD) were obtained by the crystallization of the aforementioned yellow mixture at −20 °C (see the Experimental section for details). As shown in Fig. 2, the SCXRD of Cu_{10} revealed that it crystallized in the $P\bar{1}$ space group (Tables S1–3†) and there were two non-equivalent Cu_{10} clusters in the unit cell, denoted as $Cu_{10}\text{-}a$ and $Cu_{10}\text{-}b$, respectively (Fig. 2a and S1–3†). Both of them are composed of ten Cu^+, six Pz^-, six $PhC≡C^-$ and two positively charged Et_3NH^+ molecules, resulting in neutral clusters with the mole-
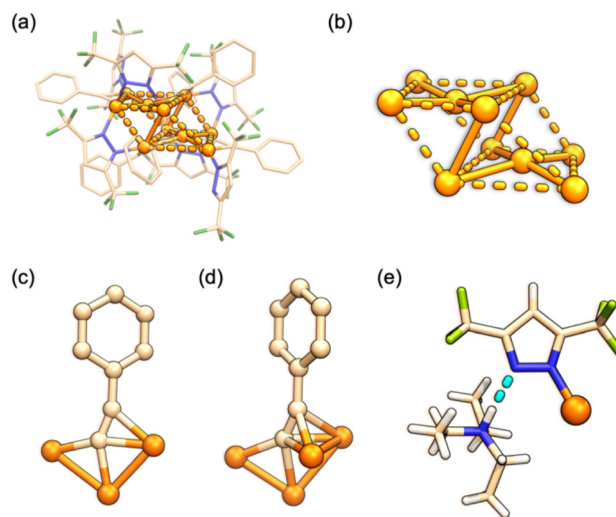
Fig. 2 The crystal structure of Cu_{10} (only structures of $Cu_{10}\text{-}a$ are shown for clarity). (a) Overall structure; (b) metal core and (c) and (d) ligation modes of an alkyne and (e) the monodentate mode and hydrogen bonding of Pz^-.

cular formula $[Cu_{10}(Pz)_6(PhC≡C)_6]^{2-}(Et_3NH)^+_2$ (Fig. S2†). Several differences were observed between $Cu_{10}\text{-}a$ and $Cu_{10}\text{-}b$ including $Cu···Cu$ ($d_{Cu–Cu}$), $Cu···C$ ($d_{Cu–C}$), and $Cu···N$ ($d_{Cu–N}$) distances (Table S2†). Specifically, the copper(I) core of Cu_{10} adopts a parallelepiped-like conformation (Fig. 2b), and all Cu atoms exhibit the tridentate mode with $d_{Cu–Cu}$ in the range of 2.491–2.741 Å for $Cu_{10}\text{-}a$ and 2.503–2.671 Å for $Cu_{10}\text{-}b$ (Table S2†), respectively, indicating a strong cuprophilic interaction.[17] Compared to the previously reported bimetal clusters, in which only σ donating complexations were found,[26,28] the $PhC≡C^-$ of Cu_{10} not only shows σ donating complexations but also demonstrates a π-bonding property, leading to a more complex structure. Among the six alkyne ligands, four were found to adopt a $μ_3\text{-}η^1_σ$, $η^1_σ$, and $η^2_π$ ligation mode (Fig. 2c), while the other two take a $μ_4\text{-}η^1_σ$, $η^1_σ$, $η^2_π$, and $η^2_π$ mode (Fig. 2d). In addition, the σ-type $d_{Cu–C}$ ranged from 1.955 to 2.197 Å for $Cu_{10}\text{-}a$ and from 1.925 to 2.210 Å for $Cu_{10}\text{-}b$ (Table S2†), respectively. As for the π-type bonding mode, the $d_{Cu–C}$ distances are in the range of 2.028–2.243 Å for $Cu_{10}\text{-}a$, and 2.024–2.299 Å for $Cu_{10}\text{-}b$ (Table S2†), respectively, which are consistent with previous reports.[5,35] In addition, the Cu–N distances of $Cu_{10}\text{-}a$ and $Cu_{10}\text{-}b$ are found to be 1.939–1.994 Å and 1.931–1.995 Å, respectively (Table S2†). Furthermore, it is wort mentioning that four pyrozolate anions were observed to coordinate with two Cu^+ cations in the $μ_2$ binding mode, while two Pz^- assume a monodentate mode to complex with one Cu^+, which is rarely observed in copper metal clusters (Fig. 2e). More importantly, the strong intermolecular hydrogen bonding interactions with rather short distances between the Et_3NH^+ counter cation and uncoordinated N of monocoordinated pyrozolate (e.g., 1.915 and 1.926 Å for $Cu_{10}\text{-}a$ and $Cu_{10}\text{-}b$, respectively) are observed (Fig. S3†). Moreover, the DCM molecules have been incorporated during crystallizations (Fig. S1†),

This journal is © the Partner Organisations 2022

Inorg. Chem. Front., 2022, **9**, 5327–5334 | **5329**

and **Cu$_{10}$** displays an ABAB-type packing mode, while being viewed from the *a*, *b* and *c* axes (Fig. S4†).

The solution structure of **Cu$_{10}$** is characterized by ^{1}H and ^{19}F NMR analyses (Fig. S5–7†), and from its electrospray ionization mass spectrum (ESI-MS) (Fig. S8–10†). The ^{1}H NMR spectrum of **Cu$_{10}$** in CD$_2$Cl$_2$ exhibited very broad aromatic peaks for protons in PhC≡C$^-$ and Pz$^-$, and Et$_3$NH$^+$ can be observed clearly (Fig. S5†). More importantly, the ^{19}F NMR spectrum of **Cu$_{10}$** revealed three non-equivalent signals and one peak located at −60.67 ppm (Fig. S7†), which can be assigned to CF$_3$ groups on the Pz$^-$ with μ$_2$ binding mode. The other two peaks located at −60.96 and −61.36 ppm can be attributed to the CF$_3$ on the monocoordinated pyrozolate ligand (Fig. S7†). Furthermore, although the monodispersed cluster cannot be observed in the ESI-MS spectrum of **Cu$_{10}$** due to decomposition or dissociation (Fig. S8 and 9†), an intense peak at *m/z* = 102.1348 can be found in the positive mode, which matched well with the simulation for Et$_3$NH$^+$ cations (Fig. S10†). These results are highly consistent with the SCXRD structure of **Cu$_{10}$** and further confirmed the existence of the monocoordinated pyrozolate ligand and Et$_3$NH$^+$ cations.

Considering the unsaturated pyrozolate ligands, we envisioned that the **Cu$_{10}$** is able to take up more copper cations, leading to larger copper nanoclusters. Thus, we initially attempted to increase the amount of Cu$_3$Pz$_3$ (from 0.3 mmol to 0.6 mmol) during the synthesis of **Cu$_{10}$** or add other copper sources (*i.e.*, Cu[(CH$_3$CN)$_4$BF$_4$] and Cu[(CH$_3$CN)$_4$PF$_6$]) to the DCM solution of **Cu$_{10}$**, but only crystals of **Cu$_{10}$** were obtained. Surprisingly, when the crystals of **Cu$_{10}$** were dissolved in an *n*-hexane/DCM mixed solution (v/v = 29 : 1), deep orange block-like crystals of **Cu$_{18}$** were isolated, illustrating the structural transformation induced by *n*-hexane. A similar solvent-driven structural transformation was also revealed by Wang and co-workers.[36] SCXRD revealed that **Cu$_{18}$** crystalized in the *P*2$_1$/*n* space group (Tables S1 and S3†), and contained eighteen Cu$^+$, six Pz$^-$, twelve PhC≡C$^-$, and two DCM in the unit cell, resulting in a natural Cu(I) nanocluster with a formula of Cu$_{18}$Pz$_6$(PhC≡C)$_{12}$·2DCM. Unlike Pz$^-$ in **Cu$_{10}$**, all the Pz$^-$ ligands in **Cu$_{18}$** adopt a bidentate mode with d_{Cu-N} in the range of 1.891–2.017 Å. The overall structure is depicted in Fig. 3a, and its Cu core features an hourglass-like configuration (Fig. 3b). The Cu$^+$ ions adopt a tridentate mode with d_{Cu-Cu} ranging from 2.491 to 2.733 Å, indicating strong Cu···Cu interactions (Table S3†). Interestingly, besides the observed coordination mode of alkynes in **Cu$_{10}$** (Fig. 3c and d), **Cu$_{18}$** exhibits two additional types of ligation modes, namely, μ$_3$-η^1$_σ$, η^2$_π$, η^2$_π$ (Fig. 3e) and μ$_4$-η^1$_σ$, η^1$_σ$, η^1$_σ$, η^1$_σ$ (Fig. 3f). The σ-type and π-type d_{Cu-Cu} distances are found to be 1.852–2.428 Å and 2.023–2.509 Å, respectively (Table S3†).

The solution structure of **Cu$_{18}$** is also characterized by ^{1}H and ^{19}F NMR, and ESI-MS experiments. The ^{1}H NMR spectrum of **Cu$_{18}$**, similar to that of **Cu$_{10}$**, exhibited broad aromatic peaks for protons in PhC≡C$^-$ and Pz$^-$. In addition, the ^{19}F NMR spectrum of **Cu$_{18}$** revealed only one peak located at −60.67 ppm (Fig. S7†), suggesting that all CF$_3$ groups on Pz$^-$ are chemically equivalent. Several peaks are observed in the
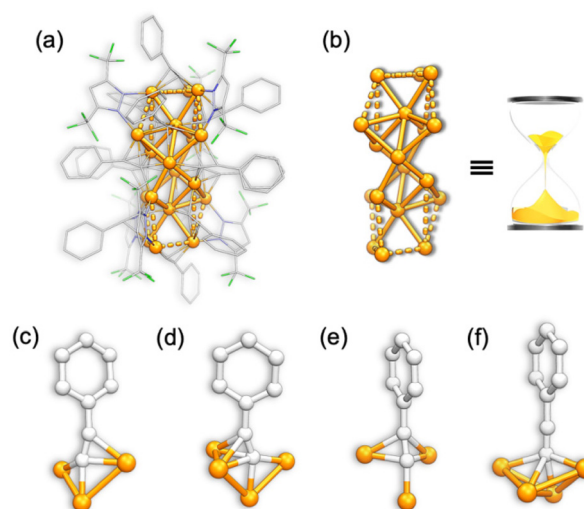
Fig. 3 The crystal structure of **Cu$_{18}$**. (a) The overall structure; (b) metal core and (c), (d), (e) and (f) four types of ligation mode of an alkyne in **Cu$_{18}$**.

ESI-MS spectrum of **Cu$_{18}$** and can be assigned to the fragments of **Cu$_{18}$** (Fig. S9†). Moreover, the peak of the entire **Cu$_{18}$** with Na$^+$ is also observed at *m/z* = 3598.9668. That Et$_3$NH$^+$ cations do not exist in **Cu$_{18}$** was confirmed by the NMR and ESI-MS spectra, and these data further matched well with the SCXRD structure of **Cu$_{18}$**.

The purity of **Cu$_{10}$** and **Cu$_{18}$** were further confirmed by elemental analysis and powder X-ray diffraction (see the ESI† for details and Fig. S11 and S12†). Fourier transform infrared spectroscopy (FT-IR) verified the existence of C≡C at 1980 cm^{-1} (Fig. S13†), and the subtle shift of wavenumbers relative to the standard vibration of C≡C (2100–2270 cm^{-1}) was attributed to a coordinative interaction, which was also observed in other reported alkyne–metal clusters.[37] Meanwhile, X-ray photoelectron measurements were performed to determine the valence of copper ions. The binding energy for Cu 2p$_{3/2}$ of **Cu$_{10}$** and **Cu$_{18}$** is located at 933.38 and 932.93 eV, respectively, similar to other Cu(I) complexes and no satellite peaks are observed,[38] suggesting that all Cu have a +1 valence in both clusters (Fig. S14†). The thermogravimetric analysis (TGA) clearly revealed that **Cu$_{18}$** started to decompose at 127 °C and exhibited higher thermal stability than **Cu$_{10}$** (~72 °C) (Fig. S15†). Et$_3$NH$^+$ cations of **Cu$_{10}$** are easily lost in TGA measurement, while no Et$_3$NH$^+$ cations were observed in **Cu$_{18}$**. The experimental weight loss of **Cu$_{10}$** (80%) was consistent with the theoretical value (79%), implying that all Cu(I) turns into elemental copper(0). In contrast, the experimental weight loss of **Cu$_{18}$** (50%) is lower than the theoretical value (68%). This result indicated that unknown Cu compounds perhaps were formed which can resist high temperatures even up to 800 °C.

Photophysical properties

With two novel alkynyl-protected CuNCs in hand, the photophysical properties of **Cu$_{10}$** and **Cu$_{18}$** were investigated.

5330 | *Inorg. Chem. Front.*, 2022, **9**, 5327–5334

This journal is © the Partner Organisations 2022

The solid-state UV-Vis spectra of Cu_{10} and Cu_{18} displayed strong and broad absorption bands at 317 and 348 nm, showing yellow-green and orange-red colors, respectively (Fig. 4a). As shown in Fig. 4b, the solid-state photoluminescence (PL) spectrum of Cu_{10} at room temperature (rt) displayed a strong green emission with a main peak at 514 nm, a shoulder peak at 556 nm and a broad peak at 695 nm upon excitation at 400 nm. The lifetime (τ) of these three peaks is at the microsecond scale with an average value of 8.4 μs, indicating the emission origin is the triplet state and its phosphorescent nature (Table S4 and Fig. S16†). In addition, the absolute PLQY of Cu_{10} is found to be ~35%. As for Cu_{18}, under excitation at 500 nm, it exhibited an intense orange-red emission color centered at 620 nm with a PLQY of 63% and τ_{av} = 2.8 μs (Table S4 and Fig. S16†).

Such a remarkable bathochromic shift of the emission wavelength can be attributed to the increment of the Cu contribution in the triplet state. As depicted in Fig. 1, after summarizing all reported atomically precise CuNCs, including protected S^-, P^- and I ligands (squares) and $C\equiv C^-$ (pentagons), it is worth noting that on account of the high PLQY and short lifetime, the k_r of Cu_{18} is estimated to be 2.2×10^5 s^{-1}, which exceeds most atomically precise CuNCs and is comparable to that of noble metals such as Pt and Ir, rendering it with an excellent PL efficiency (Table S5†). It is well-known that it is hard to realize a high PLQY in a low-energy emission due to the energy gap law,[39] thus orange emissive Cu_{18} represents a rare case in alkynyl-protected coinage metal clusters. Compared to most alkynyl-protected CuNCs,[5] the superior performance of Cu_{10} and Cu_{18} could be the result of tight packing and strong supramolecular interactions including C–H⋯π interactions and hydrogen bonding interactions (Fig. S17†), which are beneficial for restricting intramolecular rotation,

thus effectively decreasing nonradiative decay. To verify our hypothesis, Cu_{10} and Cu_{18} (1×10^{-5} M) were dissolved in DCM under a N_2 atmosphere, and no PL was observed. This phenomenon suggests that the PL of the single cluster molecule can be quenched effectively in the absence of supramolecular interactions.

Upon cooling from 300 K to 77 K (Fig. 4c and d), the solid-state emission intensity of Cu_{10} and Cu_{18} was enhanced gradually, along with an increment of the lifetime (Fig. S16†), indicating that the energy loss caused by a nonradiative transition had reduced. Of note, the maxima emission band of Cu_{10} is temperature-independent, in which the main peak at 514 nm, shoulder peak at 556 nm and broad peak at 695 nm were still observed at 77 K, similar to emission spectra at room temperature. As for Cu_{18}, it shifted from 620 nm (300 K) to 644 nm (77 K) during cooling processes, which is ascribed to the cluster-centered triplet state (^3CC) emission induced by the shortening of the Cu⋯Cu distance. The disagreement of temperature-dependent emission spectra of Cu_{10} and Cu_{18} implied different emission mechanisms. To verify their potential for solution-processed OLEDs, two polymethyl methacrylate (PMMA) films with 15 wt% of Cu_{10} or Cu_{18} were fabricated (Fig. S18†). Clearly, the maxima emission bands of both clusters in PMMA films (λ_{em} = 610 nm for the Cu_{10} film; λ_{em} = 660 nm for the Cu_{18} film) are red-shifted relative to those in crystalline form along with a prolonging of the lifetime (τ_{av} = 17.3 μs for the Cu_{10} film; τ_{av} = 4.4 μs for the Cu_{18} film), and a similar behavior was also observed in other coinage metal complexes.[40]

Theoretical calculation

To further elucidate the PL mechanism, density functional theory (DFT) and time-dependent density functional theory (TDDFT) calculations were subsequently performed based on the optimized structure at the ground state (see the ESI† for details). The simulated UV-Vis of Cu_{10} and Cu_{18} featured a strong absorption regime ranging from 300 to 500 nm, which is well consistent with their experimental solid-state UV-Vis spectra (Fig. S19†). Moreover, low energy absorption bands of Cu_{10} and Cu_{18} are assigned to the electronic transition $S_0 \rightarrow S_1$ (Fig. 5a, and S19†) according to the results of calculations. Apparently, Pz^- of Cu_{10} is considered to contribute more to the holes and electrons of S_1 relative to Cu_{18} as revealed by the natural transition orbitals (NTOs) (Fig. S20†), implying that the Pz^- ligand plays a more important role in the absorption of Cu_{10}, which further illustrates that the photophysical process can be effectively affected by the structural transformation (Fig. S20†). In addition, the Kohn–Sham orbitals of Cu_{10} and Cu_{18} were obtained by the DFT method based on their optimized crystal structures. In Fig. 5, in the Cu cluster core, $PhC\equiv C^-$ and Pz^- ligands both contribute to the occupied molecular orbitals of Cu_{10}, while the unoccupied molecular orbitals of Cu_{10} are mainly located on the alkyne ligand with minor contributions from Cu ions and Pz^- ligands (Fig. 5a and S21†), suggesting that the low-energy excited state of Cu_{10} is composed of a major metal–ligand charge-transfer triplet
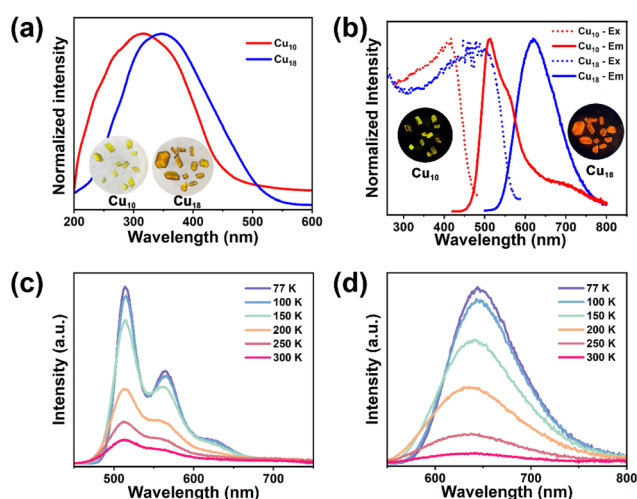
Fig. 4 Solid-state UV-Vis absorption (a), and excitation and emission spectra (b) of crystalline powders of Cu_{10} and Cu_{18}. Insets are Cu_{10} and Cu_{18} irradiated by ambient light and a hand-held UV lamp. Temperature-dependent emission spectra of Cu_{10} at λ_{ex} = 420 nm (c) and Cu_{18} at λ_{ex} = 500 nm (d).
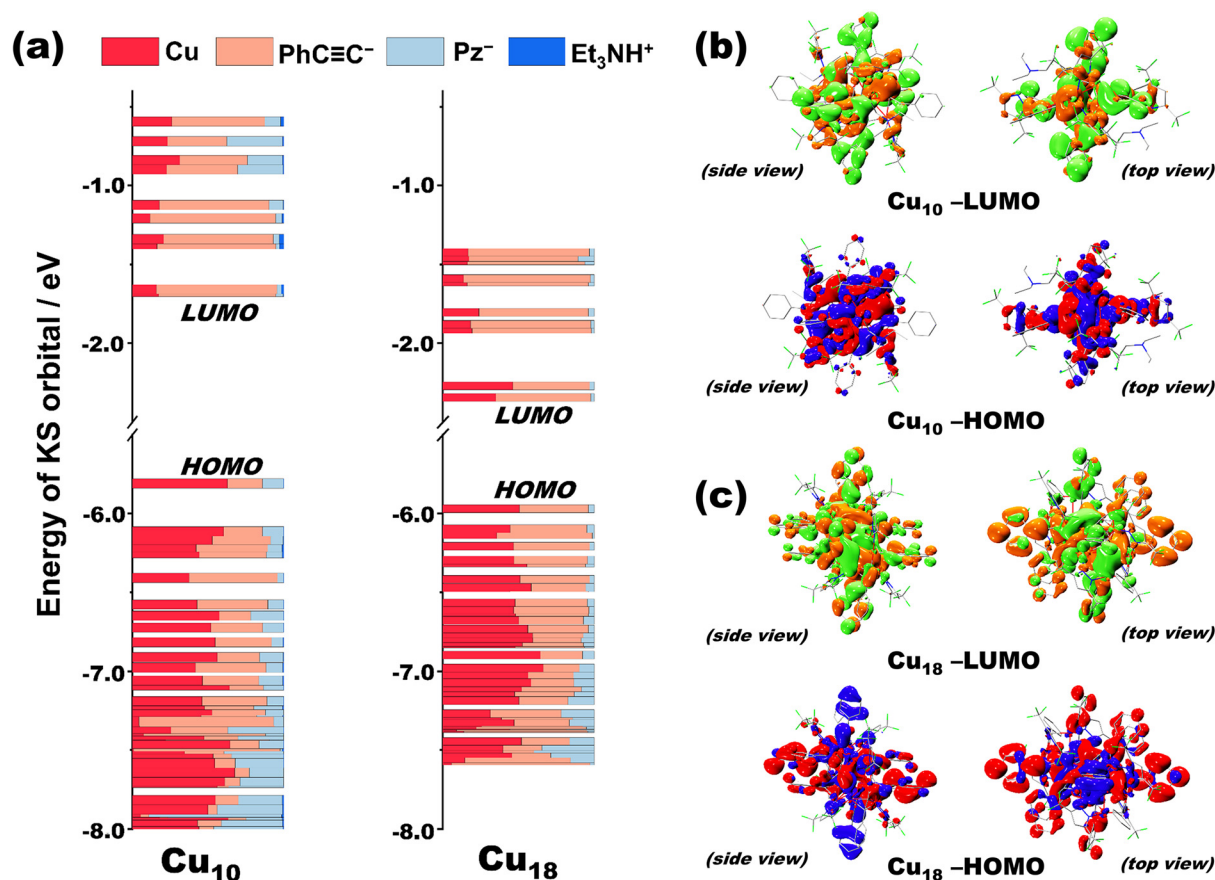
Fig. 5 Composition analysis of Kohn–Sham orbitals of **Cu₁₀** and **Cu₁₈**. (a) Electronic density diagrams of the HOMO and LUMO of (b) **Cu₁₀** and (c) **Cu₁₈** (side view and top view). H atoms are omitted for clarity.

state (^{3}MLCT) characteristic and minor ligand centered triplet state (^{3}LC) and ^{3}CC characteristics. In sharp contrast, in **Cu₁₈** clusters, the contribution of the Cu cluster core in the lowest unoccupied molecular orbitals (LUMO) is significantly enhanced, while the contribution of Pz$^-$ ligands is negligible whether in occupied molecular orbitals or unoccupied molecular orbitals (Fig. 5a and S22†). Thus, the emission of **Cu₁₈** can be assigned to the ^{3}CC and ^{3}LC emission, and due to the improvement of the metallic contribution, a great red-shift of the emission wavelength of **Cu₁₈** (λ_{em} = 620 nm) compared to **Cu₁₀** (λ_{em} = 514 nm) is observed. More importantly, the computed HOMO–LUMO gap of **Cu₁₈** (3.6273 eV) was significantly smaller than that of **Cu₁₀** (4.1361 eV) (Fig. 5a) and was also consistent with the bathochromic shift of the absorption and emission of **Cu₁₈** (Fig. 4a and b). Meanwhile, the trend that the gap of **Cu₁₈** < **Cu₁₀** was coincident no matter whether from the experimental solid-state UV-Vis diffuse reflectance spectroscopies (Fig. S23†) or calculated results. Furthermore, as shown in Fig. 5b and c, the better localization of the frontier molecular orbital in **Cu₁₈** (Fig. 5c) could induce a larger transition dipole moment than that in **Cu₁₀** (Fig. 5b), which improves the PL efficiency and absorption ability. Such theoretical results are well in agreement with the experimental data that **Cu₁₈** exhibits higher absorption ability (Fig. S24†) and

higher PLQY (Table S4†) than **Cu₁₀**. Above all, the higher d orbital contribution of the Cu cluster core, larger transition dipole moment, and smaller HOMO–LUMO gap give rise to the better PL properties of **Cu₁₈** than those of **Cu₁₀**.

Conclusions

In summary, we synthesized a parallelepiped-like and intensely green emissive **Cu₁₀** cluster from a simple Cu(ı)-CTC. **Cu₁₀** can transfer to larger alkynyl-protected CuNCs, namely **Cu₁₈**, *via* a solvent-induced structural transformation. It is noteworthy that the **Cu₁₈** not only shows a higher PLQY (35% for **Cu₁₀**, 63% for **Cu₁₈**) but also exhibits a shorter lifetime in the region of orange light (8.4 µs for **Cu₁₀**, 2.8 µs for **Cu₁₈**), thereby realizing a high k_r of *ca.* 2.2×10^5 s^{-1}. Such an excellent PL property of the **Cu₁₈** cluster exceeds that of most atomically precise CuNCs, and endows **Cu₁₈** as a suitable phosphorescent emitter for phosphorescent OLEDs. The experimental and theoretical calculations reveal the high PL efficiency of **Cu₁₈** is attributed to (i) the reduced nonradiative transition through tight packing and strong supramolecular interactions including C–H···π interactions and hydrogen bonding interactions, (ii) the larger d orbital contribution of Cu ions in the

5332 | *Inorg. Chem. Front.*, 2022, **9**, 5327–5334

This journal is © the Partner Organisations 2022

unoccupied orbital, (iii) an enhanced transition dipole moment, and (iv) a reduced HOMO–LUMO gap. Our investigations will arouse the interest of related researchers in synthesizing highly photoluminescence efficient alkyne Cu clusters. Further studies for using **Cu₁₈** as the emission layer to fabricate OLED devices are underway.

Conflicts of interest

There are no conflicts to declare.

Author contributions

G.-H. Ning, D. Li, S.-K. Peng and H. Yang conceptualized the methodology of this project, wrote the original draft and revised it. S.-K. Peng and H. Yang conducted the experiments and theoretical calculations. G.-H. Ning, D. Li, S.-K. Peng, H. Yang, D. Luo, M. Xie and W.-J. Tang performed data analysis. G.-H. Ning and D. Li supervised the whole project. All the authors have read and commented on the manuscript.

Acknowledgements

References

1 R. Jin, C. Zeng, M. Zhou and Y. Chen, Atomically precise colloidal metal nanoclusters and nanoparticles: fundamentals and opportunities, *Chem. Rev.*, 2016, **116**, 10346–10413.

2 Q. Yao, T. Chen, X. Yuan and J. Xie, Toward total synthesis of thiolate-protected metal nanoclusters, *Acc. Chem. Res.*, 2018, **51**, 1338–1348.

3 S. Wang, Q. Li, X. Kang and M. Zhu, Customizing the structure, composition, and properties of alloy nanoclusters by metal exchange, *Acc. Chem. Res.*, 2018, **51**, 2784–2792.

4 Z. Han, X.-Y. Dong, P. Luo, S. Li, Z.-Y. Wang, S.-Q. Zang and T. C. W. Mak, Ultrastable atomically precise chiral silver clusters with more than 95% quantum efficiency, *Sci. Adv.*, 2020, **6**, eaay0107.

5 M.-M. Zhang, X.-Y. Dong, Y.-J. Wang, S.-Q. Zang and T. C. W. Mak, Recent progress in functional atom-precise coinage metal clusters protected by alkynyl ligands, *Coord. Chem. Rev.*, 2022, **453**, 214315.

6 B. Li, H.-T. Fan, S.-Q. Zang, H.-Y. Li and L.-Y. Wang, Metal-containing crystalline luminescent thermochromic materials, *Coord. Chem. Rev.*, 2018, **377**, 307–329.

7 M.-M. Zhang, K. Li and S.-Q. Zang, Progress in Atomically Precise Coinage Metal Clusters with Aggregation-Induced Emission and Circularly Polarized Luminescence, *Adv. Opt. Mater.*, 2020, **8**, 1902152.

8 J. J. Pelayo, I. Valencia, A. P. García, L. Chang, M. López, D. Toffoli, M. Stener, A. Fortunelli and I. L. Garzón, Chirality in bare and ligand-protected metal nanoclusters, *Adv. Phys.: X*, 2018, **3**, 1509727.

9 K. R. Krishnadas, L. Sementa, M. Medves, A. Fortunelli, M. Stener, A. Fürstenberg, G. Longhi and T. Bürgi, Chiral Functionalization of an Atomically Precise Noble Metal Cluster: Insights into the Origin of Chirality and Photoluminescence, *ACS Nano*, 2020, **14**, 9687–9700.

10 S. Li, X.-S. Du, B. Li, J.-Y. Wang, G.-P. Li, G.-G. Gao and S.-Q. Zang, Atom-precise modification of silver(ɪ) ligand substitution: a new approach to generation of cluster functionality and chirality, *J. Am. Chem. Soc.*, 2018, **140**, 594–597.

11 X.-K. Wan, J.-Q. Wang, Z.-A. Nan and Q.-M. Wang, Ligand effects in catalysis by atomically precise gold nanoclusters, *Sci. Adv.*, 2017, **3**, e1701823.

12 X. Liu, G. Saranya, X. Huang, X. Cheng, R. Wang, M. Chen, C. Zhang, T. Li and Y. Zhu, Dimeric assembly of Au₂₅(PET)₁₈ enabled by silver atoms, *Angew. Chem., Int. Ed.*, 2020, **59**, 13941–13946.

13 X. Du and R. Jin, Atomically precise metal nanoclusters for catalysis, *ACS Nano*, 2019, **13**, 7383–7387.

14 W. Wang, Z. Wang, D. Sun, S. Li, Q. Deng and X. Xin, Supramolecular self-sssembly of atomically precise silver nanoclusters with chiral peptide for temperature sensing and detection of arginine, *Nanomaterials*, 2022, **12**, 424.

15 A. Nag, P. Chakraborty, A. Thacharon, G. Paramasivam, B. Mondal, M. Bodiuzzaman and T. Pradeep, Atomically precise noble metal cluster-assembled superstructures in water: luminescence enhancement and sensing, *J. Phys. Chem. C*, 2020, **124**, 22298–22303.

16 V. Subramanian, S. Jena, D. Ghosh, M. Jash, A. Baksi, D. Ray and T. Pradeep, Dual probe sensors using atomically precise noble metal clusters, *ACS Omega*, 2017, **2**, 7576–7583.

17 M.-M. Zhang, X.-Y. Dong, Z.-Y. Wang, H.-Y. Li, S.-J. Li, X. Zhao and S.-Q. Zang, AIE triggers the circularly polarized luminescence of atomically precise enantiomeric copper(ɪ) alkynyl clusters, *Angew. Chem., Int. Ed.*, 2020, **59**, 10052–10058.

18 L. Shang, S. Dong and G. Nienhaus, Ultra-small fluorescent metal nanoclusters: synthesis and biological applications, *Nano Today*, 2011, **6**, 401–418.

19 R. Jin, G. Li, S. Sharma, Y. Li and X. Du, Toward active-site tailoring in heterogeneous catalysis by atomically precise metal nanoclusters with crystallographic structures, *Chem. Rev.*, 2021, **121**, 567–648.

This journal is © the Partner Organisations 2022

Inorg. Chem. Front., 2022, **9**, 5327–5334 | **5333**

20 R. Hamze, J. L. Peltier, D. Sylvinson, M. Jung, J. Cardenas, R. Haiges, M. Soleilhavoup, R. Jazzar, P. I. Djurovich, G. Bertrand and M. E. Thompson, Eliminating nonradiative decay in Cu(I) emitters: >99% quantum efficiency and microsecond lifetime, *Science*, 2019, **363**, 601–606.

21 G. U. Mahoro, J. Fernandez-Cestau, J. L. Renaud, P. B. Coto, R. D. Costa and S. Gaillard, Recent advances in solid-state lighting devices using transition metal complexes exhibiting thermally activated delayed fluorescent emission mechanism, *Adv. Opt. Mater.*, 2020, **8**, 2000260.

22 M. Olaru, E. Rychagova, S. Ketkov, Y. Shynkarenko, S. Yakunin, M. V. Kovalenko, A. Yablonskiy, B. Andreev, F. Kleemiss, J. Beckmann and M. Vogt, A small cationic organo-copper cluster as thermally robust highly photo- and electroluminescent material, *J. Am. Chem. Soc.*, 2020, **142**, 373–381.

23 Z. Han, X. Zhao, P. Peng, S. Li, C. Zhang, M. Cao, K. Li, Z.-Y. Wang and S.-Q. Zang, Intercluster aurophilicity-driven aggregation lighting circularly polarized luminescence of chiral gold clusters, *Nano Res.*, 2020, **13**, 3248–3252.

24 J. Zheng, H. Yang, M. Xie and D. Li, The π-acidity/basicity of cyclic trinuclear units (CTUs): from a theoretical perspective to potential applications, *Chem. Commun.*, 2019, **55**, 7134–7146.

25 R. Jazzar, M. Soleilhavoup and G. Bertrand, Cyclic (alkyl)- and (aryl)-(amino)carbene coinage metal complexes and their applications, *Chem. Rev.*, 2020, **120**, 4141–4168.

26 J. Zheng, J.-N. Wang, T. Wang, K. Wu, R.-J. Wei, W. Lu and D. Li, Phosphorescent metal rotaxane-like bimetallic Ag/Au clusters, *J. Phys. Chem. C*, 2021, **125**, 9400–9410.

27 Z. Lu, Y. J. Yang, W. X. Ni, M. Li, Y. Zhao, Y. L. Huang, D. Luo, X. Wang, M. A. Omary and D. Li, Aggregation-induced phosphorescence sensitization in two heptanuclear and decanuclear gold-silver sandwich clusters, *Chem. Sci.*, 2020, **12**, 702–708.

28 S.-K. Peng, Z. Lu, M. Xie, Y.-L. Huang, D. Luo, J.-N. Wang, X.-W. Zhu, X. Li, X.-P. Zhou and D. Li, Unexpected structural transformation into noria-like Ag$_{13}$ metal clusters and a copper-doping induced boost in photoluminescence, *Chem. Commun.*, 2020, **56**, 4789–4792.

29 Z.-C. Shi, W. Chen, S.-Z. Zhan, M. Li, M. Xie, Y. Y. Li, S. W. Ng, Y.-L. Huang, Z. Zhang, G.-H. Ning and D. Li, Guest effects on crystal structure and phosphorescence of a Cu$_6$L$_3$ prismatic cage, *Inorg. Chem. Front.*, 2020, **7**, 1437–1444.

30 Z.-Y. Zhang, D.-Q. Ye, Q.-Q. Gao, Z.-C. Shi, M. Xie, S.-Z. Zhan, Y.-L. Huang, G.-H. Ning and D. Li, Guest-boosted phosphorescence efficiency of a supramolecular cage, *Inorg. Chem. Front.*, 2021, **8**, 2299–2304.

31 H.-G. Zhou, R.-Q. Xia, J. Zheng, D. Yuan, G.-H. Ning and D. Li, Acid-triggered interlayer sliding of two-dimensional copper(I)–organic frameworks: more metal sites for catalysis, *Chem. Sci.*, 2021, **12**, 6280–6286.

32 R.-J. Wei, H.-G. Zhou, Z.-Y. Zhang, G.-H. Ning and D. Li, Copper(I)–organic frameworks for catalysis: networking metal clusters with dynamic covalent chemistry, *CCS Chem.*, 2021, **3**, 2045–2053.

33 J. Zheng, Z. Lu, K. Wu, G.-H. Ning and D. Li, Coinage-metal-based cyclic trinuclear complexes with metal–metal interactions: theories to experiments and structures to functions, *Chem. Rev.*, 2020, **120**, 9675–9742.

34 H. V. R. Dias, S. A. Polach and Z. Wang, Coinage metal complexes of 3,5-bis(trifluoromethyl)pyrazolate ligand: Synthesis and characterization of {[3,5-(CF$_3$)$_2$Pz]Cu}$_3$ and {[3,5-(CF$_3$)$_2$Pz]Ag}$_3$, *J. Fluor. Chem.*, 2000, **103**, 163–169.

35 X. Liu and D. Astruc, Atomically precise copper nanoclusters and their applications, *Coord. Chem. Rev.*, 2018, **359**, 112–126.

36 S.-F. Yuan, Z.-J. Guan, W.-D. Liu and Q.-M. Wang, Solvent-triggered reversible interconversion of all-nitrogen-donor-protected silver nanoclusters and their responsive optical properties, *Nat. Commun.*, 2019, **10**, 4032.

37 J.-J. Fang, Y.-L. Shen, Z. Liu, C. Liu, Y.-P. Xie and X. Lu, Copper(I) alkynyl clusters with crystallization-induced emission enhancement, *Inorg. Chem.*, 2021, **60**, 13493–13499.

38 H. Li, H. Zhai, C. Zhou, Y. Song, F. Ke, W. W. Xu and M. Zhu, Atomically precise copper cluster with intensely near-infrared luminescence and its mechanism, *J. Phys. Chem. Lett.*, 2020, **11**, 4891–4896.

39 Y.-C. Wei, S. F. Wang, Y. Hu, L.-S. Liao, D.-G. Chen, K.-H. Chang, C.-W. Wang, S.-H. Liu, W.-H. Chan, J.-L. Liao, W.-Y. Hung, T.-H. Wang, P.-T. Chen, H.-F. Hsu, Y. Chi and P.-T. Chou, Overcoming the energy gap law in near-infrared OLEDs by exciton–vibration decoupling, *Nat. Photonics*, 2020, **14**, 570–577.

40 D. Zhou, W.-P. To, Y. Kwak, Y. Cho, G. Cheng, G. S. M. Tong and C.-M. Che, Thermally stable donor–acceptor type (alkynyl)gold(III) tADF emitters achieved EQEs and luminance of up to 23.4% and 70 300 cd m^{-2} in vacuum-deposited OLEDs, *Adv. Sci.*, 2019, **6**, 1802297.

5334 | *Inorg. Chem. Front.*, 2022, **9**, 5327–5334

This journal is © the Partner Organisations 2022